

Damage Induced in α -Quartz by High-Energy Heavy Ions

Undergraduate Honors Research Thesis

University of New Mexico Physics and Astronomy Department

April 28, 2005

Student: Adam Norman
UNM Advisor: David Dunlap
SNL Advisors: David Follstaedt and Barney Doyle

Abstract

The structure of the damage tracks created in α -quartz (crystalline SiO_2) by high-energy gold ions was analyzed using transmission electron microscopy (TEM). The quartz was thinned to electron transparency with the $[2\ -2\ 3]$ axis near normal to the surface. Once thinned, the quartz was irradiated at a normal incidence with 374 MeV Au^{+26} ions. TEM examination of the damaged regions revealed that the individual ion tracks likely have an amorphous core and that the crystalline lattice around them appears to be strained radially from the track centers. A detailed description of creating and analyzing these tracks is given, and necessary background knowledge is explained as needed.

Table of Contents

1	Introduction.....	3
2	Experimental setup.....	6
2.1	Sample Preparation	6
2.2	Irradiation.....	7
2.2.1	Accelerator Description	8
3	Ion-Solid Interactions.....	10
4	Quartz Structure	12
4.1	Material Description	12
4.2	Determining Crystal Orientation.....	13
5	Basics of Transmission Electron Microscopy.....	14
5.1	Crystal Diffraction	16
5.2	Diffraction Effects in Images (2-beam Condition)	18
5.3	Image Contrast Theories	19
6	Track Analysis	19
6.1	Imaging Tracks	19
6.2	Track Model.....	20
6.3	G-Vector Perpendicular to Track - Exact Bragg Condition.....	21
6.4	G-Vector Perpendicular to Track - Near Bragg Condition.....	23
6.5	G-vector Parallel to Track - Exact Bragg Condition	24
6.6	G-vector Parallel to Track - Near Bragg Condition.....	26
7	Conclusion	26
8	Acknowledgements.....	27
	References.....	28

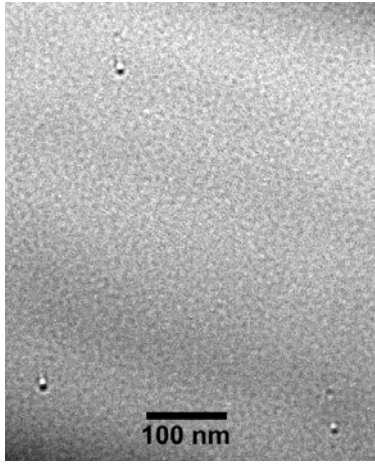


Figure 1: Tracks in sapphire created by 374 MeV Au⁺²⁶ ions. Sample is tilted 33 degrees from the incident angle of the ion. At the surface of the tracks, the black outside and white inside contrasts indicate that craters have formed.

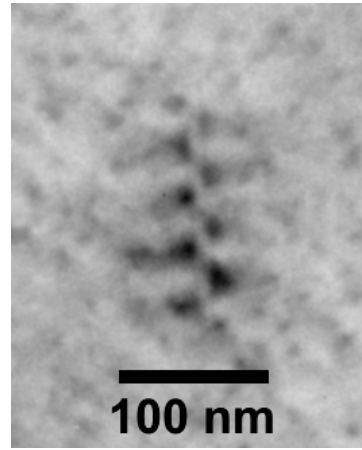


Figure 2: Track in crystalline quartz created by a 374 MeV Au⁺²⁶ ions. The sample is tilted ~35 degrees from the incident angle of the ion. Diffraction contrast shows an oscillatory pattern of black spots on either side of a lighter central region.

1 Introduction

This experimental research project took place at Sandia National Laboratories under the supervision and guidance of David Follstaedt and Barney Doyle. David Follstaedt is a transmission electron microscopist and a senior member of the technical staff. Barney Doyle is the manager of our department and specializes in accelerator-based physics. Throughout this project I regularly met with David Dunlap, my advisor at the University of New Mexico Physics and Astronomy Department, to discuss the progress of the research.

The original motivation for investigating high-energy ion tracks was to determine if nanometer-sized holes, termed “nanopores”, could be created in super-thin materials. In the past we have examined irradiated thin samples such as α -quartz, muscovite mica, and sapphire¹ (**Fig. 1**). We found ion tracks but we did not find any through-holes. In the process of trying to make nanopores, I discovered some very interesting contrast patterns in the α -quartz tracks (**Fig. 2**). In order to learn what was causing these symmetrical patterns, and to better understand the physics involved in track, surface crater, and pore formation, I performed a detailed study of the tracks in quartz using transmission electron microscopy (TEM).

I will begin by giving a brief overview of the theories of track formation and our experimental approach. High-energy ions (a few MeV/amu) that pass through solids often leave an observable damage track along the ion paths. The ions transfer large

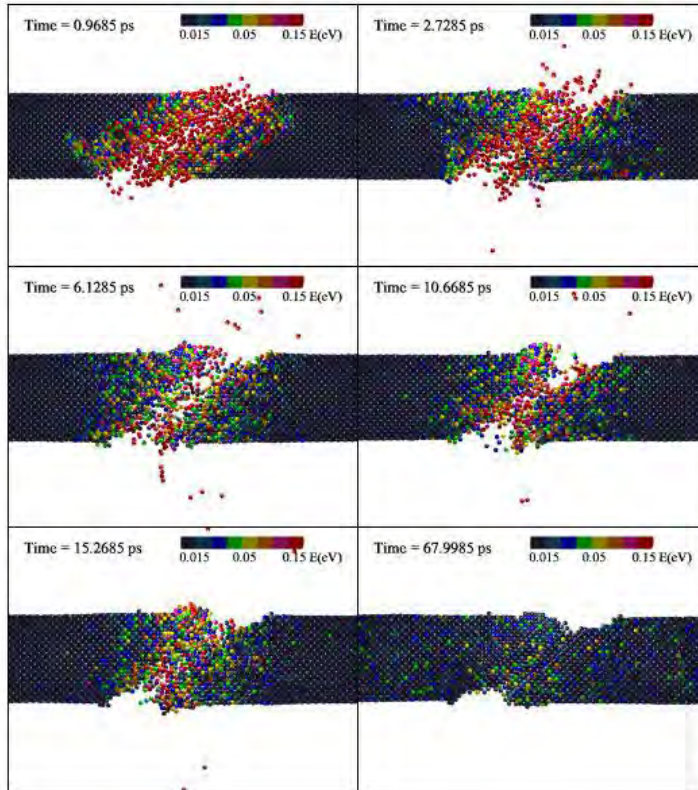


Figure 3: Molecular dynamics simulation of the disruption caused by an ion going through a thin film. This is a slice of a 3D simulation. Here the ion is assumed to deposit energy to atoms inside a cylinder of radius 1 nm along the incident track (courtesy E. Bringa of Lawrence Livermore National Labs).

amounts of energy to electrons in the target material by electronic stopping, which ionizes the target atoms along the ion tracks. There are two models often used to describe what happens next. In one, the “thermal spike” model, the material along the track is described as being heated and then interacting with its surroundings until it comes back into equilibrium^{2, 3}. The other, the “coulomb explosion” model, describes the newly created ions as being repelled from one another and moving away from the track center⁴. This ambiguity was recently resolved using molecular dynamics simulations that show when a high-energy ion passes through a material, a coulomb explosion occurs first, giving energy to the target atoms⁵. After this the ionized atoms are neutralized and interactions can be described by the thermal spike model. Thus both models appear valid in that they describe part of the physical phenomena produced by the ions.

Another feature of high-energy ions interacting with solids is that some of the target atoms are ejected from the surface because of the large amount of energy that is deposited. Investigations have shown that high-energy ions can produce craters on sample surfaces^{1, 6}. Molecular dynamics simulations also predict that craters will form, as seen in the last frame of **Fig. 3**.



Figure 4: Our 200 keV Philips CM20 Transmission Electron Microscope.

The goal of this research project was to understand the resultant structure of the tracks by using TEM. In order to investigate the structure, we used high energy ions to irradiate electron transparent specimens with thicknesses less than about 200 nm. In order to analyze the structure of the tracks, we set up various diffraction conditions by tilting the specimen to specific crystallographic orientations with respect to the incident electron beam. This produced diffraction contrast, which we used to look for lattice strain caused by atomic displacements around the track.

This work took place at the Ion Beam Materials Research Laboratory of Sandia National Laboratories (SNL). Electron transparent samples of various insulators were prepared in our TEM lab. The samples were then irradiated with 374 MeV Au⁺²⁶ ions using our tandem accelerator and a Radio Frequency Quadrupole (RFQ) linear accelerator booster. The high-energy ions lose 20-35 keV/nm along their path through these insulators, leaving behind damaged tracks. The resulting tracks were analyzed using our 200 keV TEM (**Fig. 4**). This involved using the electron diffraction pattern to tilt the specimen to specific crystallographic orientations, which brought out different contrast features in the tracks.

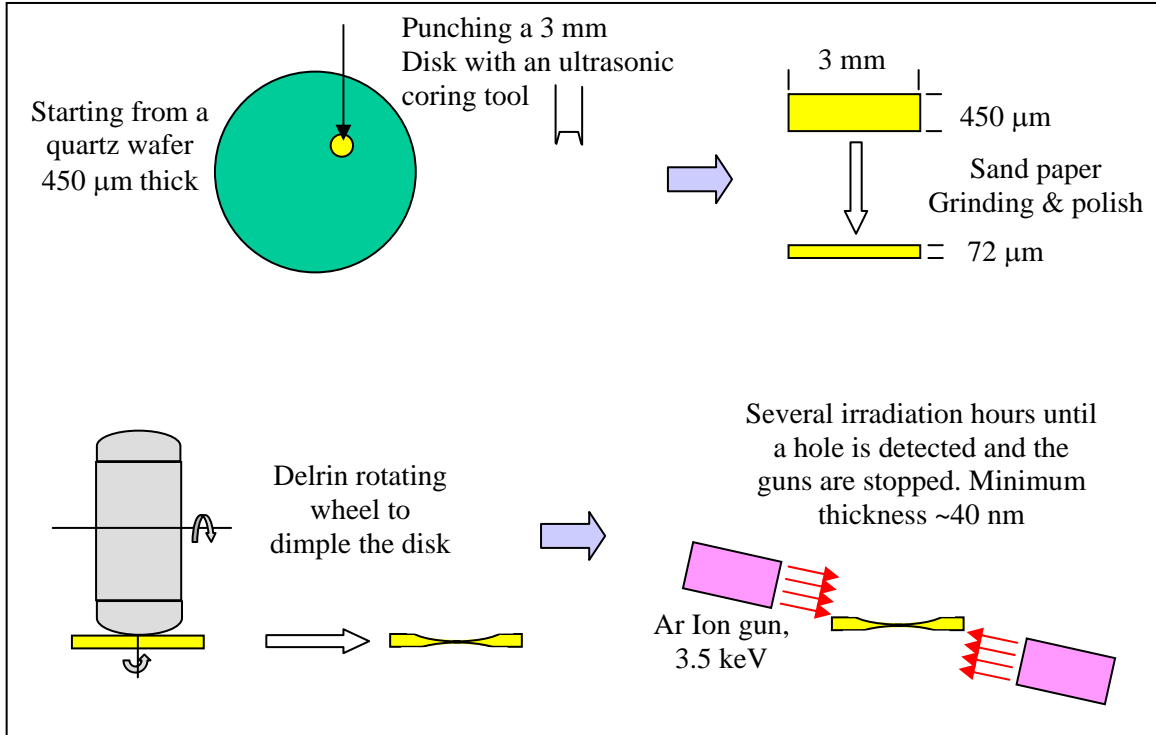


Figure 5: Preparation of an electron transparent α -Quartz sample (courtesy P. Rossi).

2 Experimental setup

As with most experimental research, much preparation was needed before we could analyze ion tracks. To begin with, an α -quartz wafer had to be acquired, which was accomplished by contacting other Sandians for available wafers. After this, the sample was made electron-transparent and then irradiated.

2.1 Sample Preparation

Preparing electron-transparent samples is an art in its own right, and each type of sample requires a different recipe. Just the right combination of techniques is needed to produce a sample with large amounts of pristine thin area. Here I will briefly describe the method I used to prepare an electron-transparent quartz sample (**Fig. 5**). After obtaining a 3-inch crystalline quartz wafer that was 450 μm thick, I used a Fischione Model 330 ultrasonic disk cutter with 15 μm boron carbide grit to core out a 3 mm disk. I then mechanically ground and polished the disk on a 5 μm aluminum oxide pad with 9 μm diamond paste until it was 72 μm thick. After this I used a Fischione Model 2000 Dimpler with a textured, rotating 15 mm diameter wheel and 1 μm diameter paste to put dimples into the top and bottom surfaces of the sample. (In a separate project, I worked with Mike Moran (SNL) to investigate this type of dimpling wheel, which he invented,

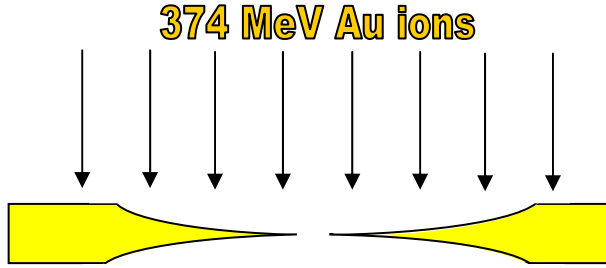


Figure 6: Cross-section of quartz sample being irradiated.

and to identify the optimum textured surface for such specimens.) Finally, I used a Gatan Model 691 Precision Ion Polishing System (an “ion mill”) to thin the central portion of the sample until a small hole formed. The ion mill works by aiming argon ions toward the sample (which is in an evacuated chamber), at a low angle relative to the plane of the sample. For this sample, I used 3.5 keV Ar ions and an angle of 4° on the top side, and 2° on the bottom side. The argon ions knock atoms off of the sample surface (this process is termed “sputtering”), and the crystal is damaged very little due to the low energy and low angle. The sample is then 72 μm thick at the supporting edge, and it tapers down to a thickness of about 40 nm around the central hole. In the TEM, the quartz needs to be thinner than approximately 200 nm to be usable. Because a small thickness gradient is produced, there is plenty of usable area.

2.2 Irradiation

Using a radio-frequency-quadrupole (RFQ) attached to a tandem accelerator, we are able to accelerate ions to very high energies of 1.9 MeV/amu (This notation is used because the RFQ accelerates ions to a fixed velocity, regardless of their mass.). After the sample was thinned, it was irradiated with 374 MeV $^{197}_{79}\text{Au}^{+26}$ ions at an incidence normal to the sample surface (**Fig. 6**). This energy corresponds to a velocity of 6.4% of the speed of light (therefore relativistic effects are negligible):

$$\text{KE} = \frac{1}{2} m_0 v^2 \Rightarrow v = (2\text{KE}/m)^{1/2} = 0.064c = 20 \text{ million km/s}$$

A fluence of about 10^8 ions per square cm (about 1 ion per square micron) was achieved after two days of irradiation. A higher fluence was not obtainable due to the popularity of the accelerator. According to an atomic simulation program called the Stopping and Range of Ions in Matter (SRIM)⁷, the gold ions deposit 24 keV/nm into the α-quartz (using its density of 2.65 g/cm³) along the ion path. The SRIM program incorporates experimental stopping power data for a large variety of materials and ions, and then it uses theory to extrapolate to unknown materials and ion-energies.

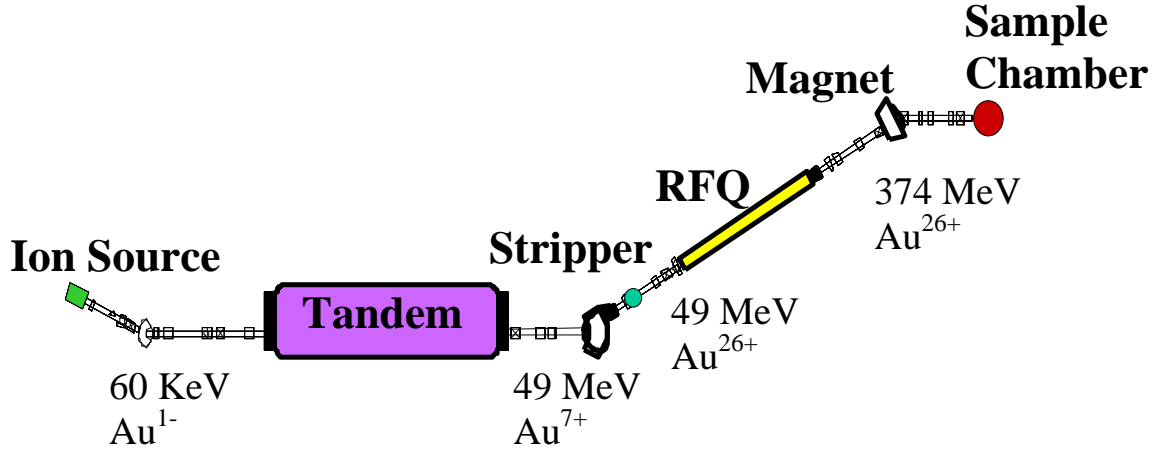


Figure 7: Our accelerator system that produces high-energy heavy ions. The tandem is about 3 meters in diameter and 13 meters long. The RFQ is 6 meters long. The total beam-line is about 40 meters in length.

2.2.1 Accelerator Description

The tandem accelerator in building 884 at Sandia has many different beam-lines, and can accelerate nearly every atom in the periodic table to a large range of energies. Here I will describe only the beam-line that pertains to accelerating Au ions (**Fig. 7**).

To begin with, Cs is heated in a reservoir, and the vapor comes out of a sintered tungsten region, which is heated to 1100°C . This high temperature tungsten strips one electron off of $\sim 99\%$ of the Cs atoms. The positive Cs ions are then accelerated through a 20 kV (from -40 kV to -60 kV) potential. At this point the Cs ions strike a source material, such as Au, and some (about 0.1%) of the source atoms are freed with a -1 charge, and accelerated to an energy of 60 keV. After this the Au ions are focused and steered by magnetic lenses. Before reaching the tandem accelerator, the beam-line turns and the strength of a steering magnet can be changed to bend the trajectory of the desired ion so that it follows the beam-line. Using the Lorentz force law, a radius of curvature r_c is obtained that depends on the magnetic field B , charge q , velocity v , and mass m . The magnetic field lines are designed to be perpendicular to the ion velocity.

$$F = qvB = \frac{mv^2}{r_c} \Rightarrow r_c = \frac{mv}{qB}$$

This is of course a simplified model that does not take into account fringing of the magnetic field. If the ion is of the wrong mass, its radius of curvature will be incorrect, so it will not successfully make the turn. After more focusing, the beam enters the tandem accelerator. The beam enters with a -1 charge, and is drawn to a +6 MV potential at the center of the tandem. At this point the beam goes through a low pressure nitrogen-filled cylinder, and electrons are stripped off the Au ions when they interact with the

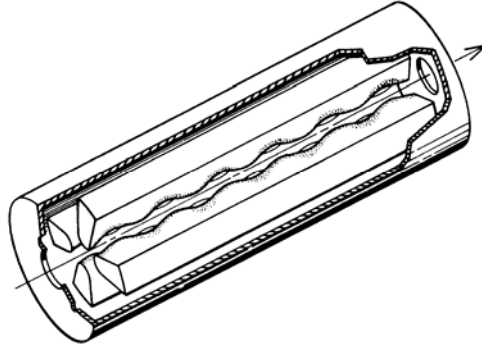


Figure 8: Cross-section of the radio-frequency-quadrupole⁸.

N_2 gas. The ions exit the N_2 -filled cylinder with a distribution of positive charges, and are accelerated to different velocities as they are now repelled by the +6 MV potential. The beam is again focused and steered. The beam-line turns again, and here 49 MeV Au^{+7} is selected by adjusting the strength of the magnets.

After being focused once again the beam passes through a carbon foil, which strips off electrons and leaves the atoms with a distribution of charges that peaks at +23. The beam then immediately enters the RFQ (**Fig. 8**). In order for the ions to be accelerated they must enter the RFQ with a velocity very close to $v_0 = 0.023c$, which corresponds to an energy near 0.25 MeV/amu. This is required so that the ions can be in resonance with the oscillating electric fields of the RFQ. In addition to this specific velocity, they must have a charge of +26 or higher so that the force on them is large enough. Only about 1% of the ions that went through the carbon foil have this large of a charge. As can be seen in **Fig. 8**, there are four metal pieces that form the beam-line. These metal pieces are each 90 degrees apart, and opposite ones are separated by about 1-3 mm. Toward the outside of the beam-line, the metal pieces are connected. The gap between opposite electrodes increases and decreases sinusoidally, with a wavelength λ that increases as the ions travel down the beam-line. This setup makes the RFQ an electromagnetic waveguide. An RF alternating current is applied at a frequency of $f = 425$ MHz, exciting the transverse electric and magnetic 210 quadrupole mode in this resonant cavity. This produces a surface charge along the beam line that alternates between positive and negative at each of the four metal tips. The undulation of neighboring electrodes is 90° out of phase, and this geometry adds a longitudinal component (to the primarily radial) electric field that accelerates ions that are in the correct time phase. The distance between the gaps continuously increases to match the increasing velocity of the accelerated ions (i.e. the alternating surface charge pushes the ions one wavelength per RF cycle, and since the wavelength increases, so does the velocity). The velocity is given by $v = \lambda f$, and the initial and final wavelengths are:

$$\lambda_0 = v_0 f = 16 \text{ mm} \qquad \lambda_f = v_f f = 45 \text{ mm}$$

With only 6 meters of RFQ beam-line, the ions are accelerated to 1.9 MeV/amu. The ions enter at a fixed velocity of 0.023c, and they exit at a fixed velocity of 0.064c. Only 10% of the ions entered at the correct time in the RF cycle and were actually accelerated. To separate the accelerated beam from the unaccelerated beam, the beam-line is turned with a magnet, and only the ions with the high-energy are magnetically selected to continue towards the target. The 374 MeV gold ions are then focused onto the sample. They pass through the sample, and each individual ion is counted by using a pin-diode and an amplifier.

Of the gold ions that are initially accelerated at the source, only about 1 in a million makes it to the sample. Most of this loss comes from the RFQ. To begin with, only 1% of the gold ions exit the carbon stripper with a high enough charge. Then, because of high power consumption, the RFQ is only on 1% of the time (it would melt if it were on for longer). For the time that it is on, only ~10% of the entering ions have the correct timing. The final 10% of the losses occurs in the tandem's stripper. Even with these losses, the flux is still high enough for most experiments. However, this particular type of experiment requires a high fluence, so 1 - 2 days of irradiation are necessary.

3 Ion-Solid Interactions

High-energy (a few MeV/amu) heavy ions incident upon a target material such as quartz are slowed down predominantly by interaction with the target electrons. Because of the high energies involved, the ions travel a considerable distance through the quartz. The average distance a 374 MeV Au ion would travel through quartz before coming to a complete stop is approximately 25 μm . The thickness of our thinned sample area is less than 0.2 μm , so very little of the ion's energy is lost before the ion exits the backside of the quartz. As stated earlier, ~24 keV of the ion's energy is lost to the quartz electrons for every nanometer the ion travels. This energy is transferred to the electrons by the coulomb interaction. Much less energy is given directly to the atomic nucleus because the energy transferred is inversely proportional to mass. This can be seen by estimating that the high-energy ion exerts a constant force F on an electron and a nucleus for a short time Δt . The impulse given to the electron/nucleus is $\Delta p = F\Delta t$. Thus the change in kinetic energy is $\Delta E = (\Delta p)^2/2m$. Because a proton is about 2000 times more massive than an electron, the electron will get much more energy. The energy given to the electrons near the incident ion is enough to free them from their parent atoms and give them additional kinetic energy. What happens next is then described by a few different models. Note that there is currently no theory that sufficiently explains all of the ion-track data.

- Thermal Spike Model

In this model the electrons do not go very far before their energy is transferred to the atomic nuclei via electron-phonon interactions. The material along the track is modeled to have an initial high temperature with a gradient that decreases as the radius from the track center increases. The heat then diffuses as described by two coupled heat-diffusion equations:

$$C_e \frac{\partial T_e}{\partial t} = \nabla(K_e \nabla T_e) - g(T_e - T_a) + B(r, t)$$

$$\rho_a C_a(T_a) \frac{\partial T_a}{\partial t} = \nabla(K_a(T_a) \nabla T_a) + g(T_e - T_a)$$

The e subscript denotes the electronic system, and the a subscript denotes the atomic system. Here, C is the specific heat, T the temperature, K the thermal conductivity, g the electron-phonon coupling constant, B the energy deposited, and ρ is the specific mass. The electron-phonon coupling constant is unknown for insulators, but can be estimated based on the mean free path of the electrons. The value of the mean free path has been estimated for a range of insulators based on experimental track radii results [12]. Plugging in the appropriate values and solving the coupled equations show that the lattice temperature of the track center drops below the melting point within about 10^{-10} s. Out to a certain radius an observable damaged region (track) is expected where the temperature exceeded the melting point of the material.^{2,3,6}

- Coulomb Explosion Model

In this model the electrons have a high kinetic energy and are able to travel a significant distance away from the track center. This leaves the track center lined with positive ions. These ions then repel each other via coulomb repulsion and move away from the track center creating a temporary void. The electrons are soon drawn back to the positive ions and the net charge is neutralized. The energy of the atoms is then radially transferred to the surrounding atoms through collisions. The timescale involved is of the same order as for the thermal spike model, and similar material properties are used.

- Atomic-Scale Simulation

Current molecular dynamics simulations (**Fig. 3**) predict that when a high-energy ion passes through a material, a coulomb explosion will occur first. Then, the ionized atoms are neutralized and interactions can be described by the random atomic motion of the thermal spike model. The simulation is set up with the following conditions: (1) The uniformly distributed atoms are initially placed in potential wells, which can be varied depending on the material being examined. (2) When the ion passes through the sample, the electrons are given a specified amount of energy depending on their

distance from the ion's path. (3) The motions of the ions that are created are then individually governed by the force exerted on them from the coulomb interaction with the other ions. Because of the number of variables in this three-dimensional model a very thin material is used (about 10 nm), resulting in the need to calculate velocities and positions for about 10^5 atoms. These simulations indicate that some aspects of each of the previous two models are important.

4 Quartz Structure

An understanding of the structure, orientation, and properties of our sample was needed before we began to analyze the tracks. Knowing the orientation and structure allowed us to set up specific diffraction conditions in the TEM. Knowing the properties helped us understand what happens when the ion deposits energy onto the sample.

4.1 Material Description

The α -quartz wafer was initially purchased from SAWYER Crystal Systems. The specified orientation was 42.75° ($\pm 0.25^\circ$) away from the hexagonal axis, about the x-axis. This corresponds to having the [2 -2 3] axis nearly normal to the surface. This orientation was used because it is a standard orientation for surface acoustic wave (SAW) applications and was readily available as a wafer. (The electronic properties of SAW wafers make them useful for many different technologies such as pressure sensitive devices⁹). The following properties were obtained from SAWYER's Material Safety Data Sheet for their cultured quartz crystal¹⁰:

Density: 2.65 g/cm^3 Melting Point: 1883 K Boiling Point: 2270 K

The crystal lattice of α -quartz is hexagonal. Every silicon atom is bonded (mostly covalently) to four oxygen atoms, which forms a tetrahedron¹¹. Every oxygen atom is bonded to two silicon atoms, thus accounting for the chemical formula SiO_2 . The following is a list of the three largest spacings of the atomic planes (d-spacings) that are readily detectable with diffraction, and the Miller indices they are associated with¹².

<u>d (Å)</u>	<u>hkl</u>
4.26	100
3.34	101
2.46	110

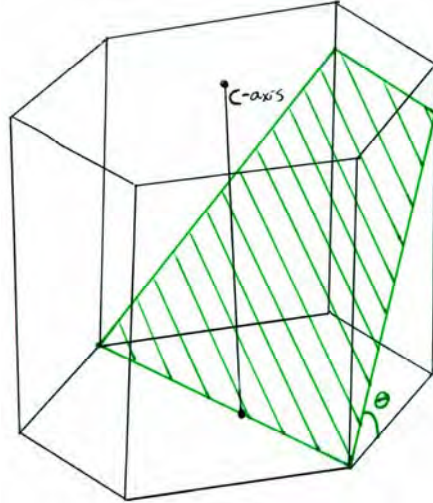


Figure 9: The c-axis is defined to be perpendicular to the hexagonal structure. Our wafer was cut as shown with $\theta = 42.75^\circ$. This cut leaves the $[2 -2 3]$ -axis nearly normal to the surface.

Our quartz was formed at a low temperature, and its structure is therefore that of the phase referred to as α -quartz. If it is heated above its melting point of 1883 K, the atoms are no longer in a crystal lattice, and rapid cooling (quenching) will freeze the atoms into place. This leaves them in a disordered (amorphous) state. Amorphous quartz, called fused silica, has a density between 2.5 and 2.65 g/cm³, with an average¹³ of 2.57 g/cm³, which is less than that of α -quartz.

4.2 Determining Crystal Orientation

To begin with, the crystal was known to be cut into wafer slices 42.75° off the c-axis (**Fig. 9**). The c-axis is normal to the hexagonal plane. To assure that I understood the orientation well, I imaged four successive diffraction patterns (discussed below) in the TEM by tilting along a single axis (**Fig. 10**). A “double tilt” specimen holder was used to provide a second tilt axis perpendicular to that of the main tilt. With this I was able to tilt about the (110) diffraction spot and keep it in place in all four images. As I tilted, I kept track of the angle the sample was tilted at. Once I had obtained the images, I indexed the diffraction patterns by measuring the reciprocal space distance to the diffraction spots and correlating them to the actual spacings of the atomic planes. With the indexed diffraction patterns, we were then able to identify the zones of the diffraction patterns, given by the crystal direction perpendicular to their plane¹⁴. The $[2 -2 3]$ zone was closest to zero tilt, and our calculations showed that this zone was 40.3° away from the c-axis, which agrees with the wafer being sliced 42.75° off the c-axis. The difference in these two angles is due to the difficulty of determining when the sample is exactly horizontal (0°) in the sample holder. Also, bending of the thin material being imaged around the hole adds error.

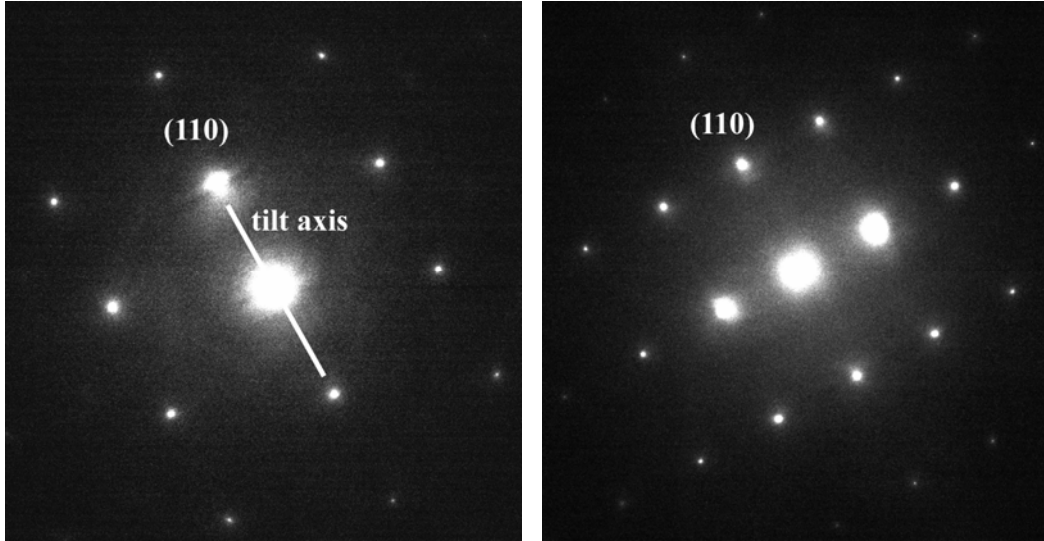


Figure 10: Two of the diffraction patterns that were used to verify the crystal orientation. The image on the left is the [2 -2 3] zone diffraction pattern and the one on the right is the [1 -1 1] zone diffraction pattern. I tilted about the labeled axis, so that the (110) spot was in all four images. These were also “landmarks” that were helpful in navigating to different crystal orientations.

5 Basics of Transmission Electron Microscopy

Before describing the results of our TEM investigations, I will briefly describe how the Philips CM20 TEM operates. To a first order approximation it is like a slide projector, except it uses electrons instead of electromagnetic waves. Electrons pass through a thin sample and exit with varying intensity depending on the internal features of the sample. An optical system focuses on the exit surface of the sample and forms an image. An added feature is that the samples have a regularly repeating atomic structure, which adds diffraction contrast. **Fig. 11** is a ray-diagram for the TEM. There are other intermediate lenses and apertures that I have left out for simplicity. To begin with, electrons are produced by heating a source. In our TEM, the source is a lanthanum hexaboride (LaB_6) crystal, which easily gives off electrons at a pointed tip when heated. The electrons are then accelerated through a 200 kV electro-static potential, and thus have a relativistic kinetic energy of 200 keV. Solving for the momentum and using the deBroglie relation, we find:

$$p = \frac{\sqrt{(200\text{keV} + mc^2)^2 - (mc^2)^2}}{c} \quad \lambda = \frac{h}{p} = 2.508 \times 10^{-12} \text{ m}$$

This wavelength gives a very small diffraction limited resolution in the picometer regime. However, the actual resolution is 2-3 Å due to spherical aberration of the TEM's objective lens¹⁵. The 200 keV electrons are guided by magnetic lenses down a chamber towards the sample. If the TEM lenses are well aligned, the electron beam is almost exactly parallel when it reaches the sample. Upon reaching the sample the electrons can

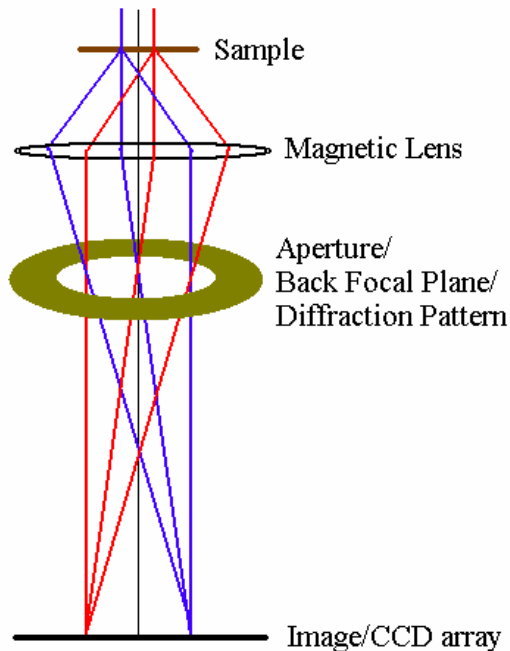


Figure 11: Simplified ray-diagram for TEM. There are other intermediate lenses and one other aperture between the aperture that is shown and the CCD array. There are also lenses above the sample which make the electron-beam parallel. The aperture is placed in the back focal plane, which is also where the diffraction pattern is located. Each spot on the diffraction pattern correlates to the direct-beam or a diffracted beam (e.g. $\theta \sim 0.2^\circ$ from $n\lambda=2d\sin\theta$). The direct-beam goes straight through the sample without being scattered or diffracted and forms the central spot. When a 2-beam condition is set up there is only the central spot and one intense diffracted spot. A smaller aperture is used which blocks the diffracted beam and only allows the direct-beam to pass through. Because the diffracted beam is blocked, areas on the sample that have diffraction will have a lower intensity in the image.

pass through the sample unaltered, they can interact inelastically, or they can interact elastically.

The unaltered beam is called the direct-beam, and its intensity is a function of the thickness, density, and composition of the sample, as well as the crystal orientation and the amount of defects. When the sample is thicker, denser, or composed of more massive elements, the intensity of the direct-beam decreases due to increased scattering. The sample may be damaged when electrons are inelastically scattered and deposit energy, especially in ionic and covalent materials like quartz¹⁵. The elastically scattered electrons produce diffraction effects, which are discussed later.

Once the electrons pass through the thin TEM sample, additional magnetic lenses are used to form a magnified image, in much the same way a light microscope forms an image. The magnetic lenses are adjusted so that the image plane of the specimen is positioned at the plane of a charge-coupled device (CCD) detector.

In addition to a magnified image, an image of the diffracted beams in reciprocal space can be obtained by focusing the back focal plane of the microscope's objective lens onto the CCD detector. The TEM does this by adjusting the strength of the magnetic lenses. The direct-beam will form a central spot, and the diffracted beams will form other spots. This image is called a diffraction pattern and its symmetry reflects that of the crystal lattice.

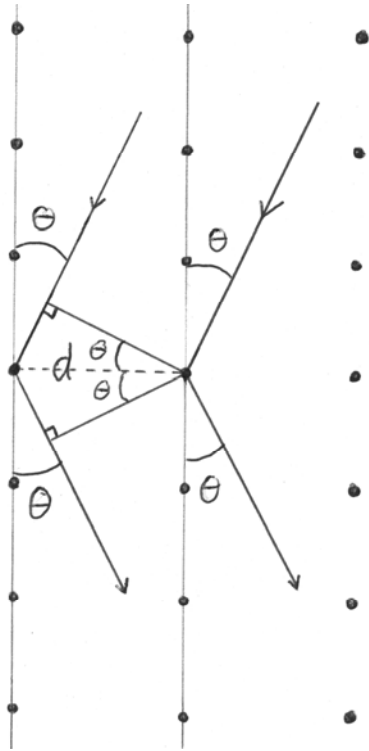


Figure 12: Illustration of Bragg's Law. The extra distance traveled on the left top side is $d\sin\theta$. This extra distance is also traveled on the left bottom side. This total extra distance traveled must be equal to an integer multiple of the electron's wavelength for there to be constructive interference: $2d\sin\theta = n\lambda$, where $n = 1, 2, 3, \dots$. When $n = 0$ there is no diffraction and the electron contributes to the direct-beam. The crystal lattice is a three dimensional structure, so electrons are diffracted at other orientations (e.g. into paper) as well.

5.1 Crystal Diffraction

Diffraction in a crystal lattice is similar to optical diffraction from slits. The TEM produces monochromatic beams in which all of the electrons have the same wavelength. The positions of maximal intensity can be found using Bragg's Law, which is $2d\sin\theta = n\lambda$. Consider two planes of atoms, spaced a distance d apart, which are vertical and going in and out of the page (**Fig. 12**). The electrons come from the top of the page, and θ is the glancing angle that the electrons make with the planes of atoms. The electrons then scatter elastically, exiting with the same angle. The difference in the distance traveled by an electron one plane of atoms over is then $2d\sin\theta$. For constructive interference this must equal an integer multiple of the electron's wavelength. As with the double-slit experiment, the distance to the screen must be much greater than the distance between the planes of atoms, so that the angle to a spot on the screen is practically the same for all of the electrons. Adding in many planes of atoms spaced a distance d apart has the same effect as adding many extra slits to the double-slit experiment (which makes a diffraction grating). The spots of maximum intensity then become more defined, and the intensity in the area between the spots goes to zero.

The direct-beam occurs when θ equals zero and there is no scattering (**Fig. 13**). The separation of the other maxima is inversely proportional to the interplanar distance d ,

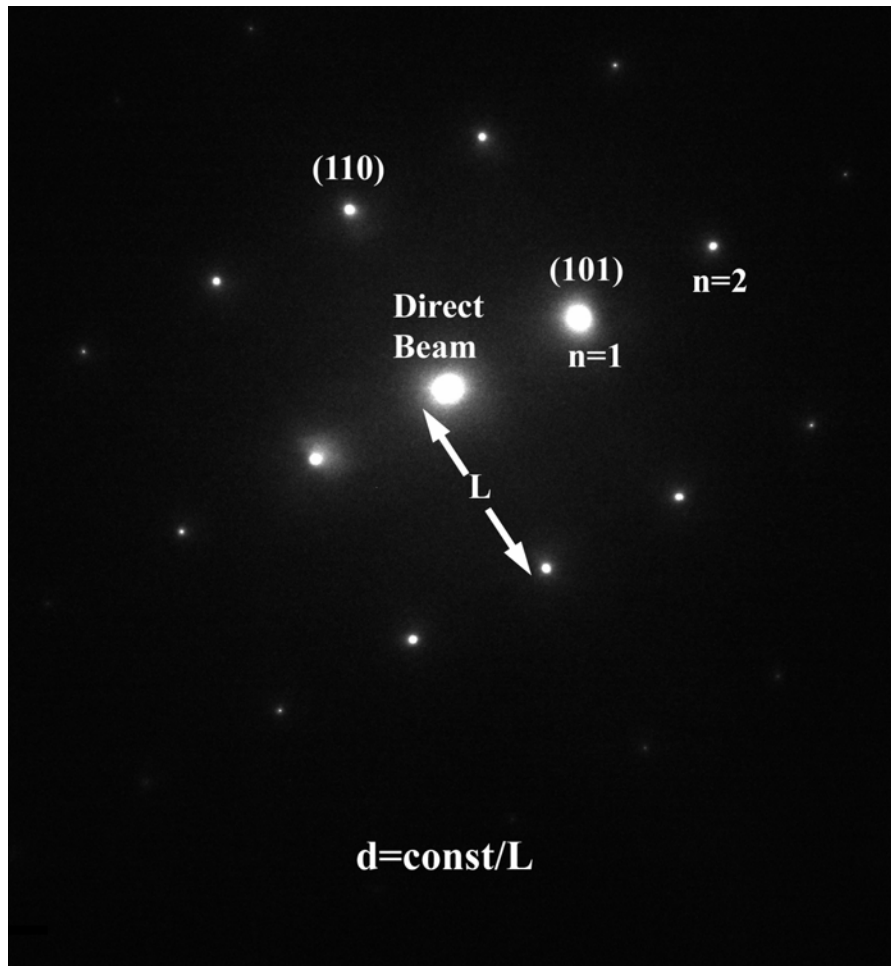


Figure 13: Diffraction pattern on the $[1 -1 1]$ zone. A vector from the direct beam to a diffracted beam is perpendicular to a plane of atoms. There are many possible vectors because the crystal is oriented so that many atomic planes satisfy the Bragg condition. The intensity of the diffracted spots indicates how close they are to the exact Bragg condition.

so the diffraction pattern is called a reciprocal-space image (just like in the double-slit experiment, where the spacing of the maxima increases when the spacing of the slits decreases). Because a crystal has many atomic planes with many symmetries, there will be scattering in other directions as well. The distance to the diffraction spot from the direct-beam is inversely proportional to the spacing of those atomic planes, and the direction is normal to the planes.

As with the double slit experiment, it does not take many atoms in the crystal lattice to produce sharp diffracted beams. Small volumes of the sample can be thought of as individual gratings, so that the sample is made up of many different “gratings”. Each of these volumes then diffracts according to its local lattice orientation to produce contrast in the image, as described below.

5.2 Diffraction Effects in Images (2-beam Condition)

When imaging in the TEM, the contrast is caused not only by inelastic scattering due to density and thickness variations, but also by the effects of the diffracted beams. The simplest (and widely used) case is when there is only one set of atomic planes that satisfies the Bragg-condition to produce strong diffraction. In the diffraction pattern, this corresponds to having the central beam and one intense diffracted spot (see **Fig. 14** for an example). A vector pointing from the main beam to the diffracted beam is called the **g**-vector. This vector points perpendicular to the atomic planes that are causing the diffraction. The higher order spots, and the spots on the opposite side of the direct-beam are minimized (i.e. we only want the $n=0$ and the $n=1$ spots). The crystal is oriented to get this 2-beam condition by tilting the sample relative to the incoming electron-beam, which changes the orientation of the atomic planes. In practice, it is difficult to get a perfect 2-beam with α -quartz. There are always other weak spots in the diffraction pattern, but if their intensities are minimized, they do not play an important role in forming the contrast of the image.

With the 2-beam condition set up, an aperture is placed in the back focal plane of the objective lens, and the direct-beam is allowed to pass through it while the diffracted beam is blocked (refer to **Fig. 11**). This type of imaging is known as “bright-field” imaging. In the image of the specimen, places where the Bragg-condition is satisfied will have lower intensity, because more electrons are diffracted out of the direct-beam and do not contribute to the image. Because TEM samples are so thin, there is always a small amount of bending in the sample. This means that only part of the crystal satisfies the Bragg-condition. This lower intensity area where the Bragg condition is satisfied is called a bend contour (and can be seen in **Fig. 15**).

When imaging on or near a bend contour, local variations in crystal orientation are seen as contrast. This is because the orientation of small crystal volumes will be locally tilted so as to either be more or less aligned with the Bragg condition. If it is more aligned, the area will be darker because the diffracted electrons will not take part in forming the image. If it is less aligned, the small volume will be brighter because there will be less diffraction. This effect is observed if the lattice is being strained.

When a crystal lattice is strained, the spacing between lattice planes is also changed. This changes the angle at which diffraction occurs because the d in Bragg’s Law changes. As a general rule, strain will make the small crystal volumes more or less aligned with the Bragg condition if the local atomic displacement **R**, is in the direction of the **g**-vector. This is because with a 2-beam condition, diffraction is only occurring for a specifically oriented set of atomic planes, so only a change in the spacing and orientation of these

planes will lead to an altered diffracted intensity. This means that the contrast will be changed the most when \mathbf{g} is parallel to \mathbf{R} . This is known as $\mathbf{g} \bullet \mathbf{R}$ (\mathbf{g} dot \mathbf{R}) contrast¹⁵.

5.3 Image Contrast Theories

In my analysis of the ion tracks I will refer to the kinematical and dynamical theories of image contrast in the TEM. The kinematical theory is an approximation of TEM contrast and can be used to qualitatively understand contrast¹⁶. It assumes that most of the intensity of the incident beam remains in the direct beam. If the kinematical theory does not fully explain the contrast, or if a quantitative explanation is needed, the dynamical theory of TEM contrast must be used. The dynamical theory often uses solutions to the Schrödinger wave equation for the incoming, transmitted, and diffracted electrons¹⁶. It takes into account the fact that the diffracted beam may also scatter, either back into the direct beam or in a different direction. In most of our images, the kinematical theory sufficiently explains the contrast. However, the dynamical theory must also be used to explain a few other features.

6 Track Analysis

Enough background information has now been given so that the reader can understand the track images. Throughout the course of this research project I imaged about 30 tracks with various tilts and \mathbf{g} -vectors. We quickly realized that each \mathbf{g} -vector produced a distinct set of features, and that imaging multiple tracks only led to new information if the sample had been damaged around a previously imaged track. After giving an overview of imaging tracks, I will present a model that appears to explain the contrast in all of the track images. Then I will describe the results obtained from imaging the tracks under four different diffraction conditions.

6.1 Imaging Tracks

Due to several complicating factors, it is difficult to obtain high-quality images of the tracks in α -quartz. To begin with, the tracks are very small, with a diameter of about 10 nm. Also, they exhibit weak contrast under most diffraction conditions. A third problem is that there is only about one track in every square micron. At the magnification needed to detect the tracks, their separation is more than one image width. In order to overcome these problems, I tilt the sample approximately 30°. While looking at the microscope's viewing screen, I slowly tilt the sample so that different diffraction contours pass through the area I am looking at (as the Bragg condition is satisfied for different atomic planes).

If there is a track, I will see its contrast change as it approaches, enters, and leaves a bend contour. If I do not see a track, I can translate the specimen to a new area and rapidly search for another track. Using this method, I can quickly locate a track.

This approach is complicated by the fact that I need to have the crystalline material around the track in the correct 2-beam condition. In order to accomplish this, I begin by setting up the proper 2-beam condition, and then I switch to dark-field (DF) imaging. This condition is achieved by tilting the incoming electron beam so that the diffracted beam passes through the objective aperture and down the microscope's optic axis for sharp imaging. Now, instead of seeing a bright screen with dark bend-contours, you see a dark screen with one bright bend-contour. This is the area where the Bragg-condition is satisfied. I can now look in this area for the tracks. By searching in this bright band and tilting, I am able to locate the tracks and remain in the correct 2-beam condition. However, because I only have one diffracted beam to work with, it is more difficult to find tracks using this method than using the method described in the previous paragraph.

To make matters worse, α -quartz is easily damaged by the electron-beam. This problem has also been documented by others¹⁷. When I finally find a track and take two images 60 seconds apart while leaving the beam on, the area shows damaged spots and the track's appearance has changed! To counter this effect, I search with very low beam intensity. I also converge the beam, so that only a small portion of the sample is being damaged at one time. When I find a track, I increase the intensity for a short time (about 10 seconds) when taking an image. By working quickly I can find and image a track before it has changed noticeably. I know it has not changed significantly because the beam is over the track for only a short time before I image it, and the track remains stable for several subsequent images.

6.2 *Track Model*

Based on track research by Meftah et al¹⁸, it is expected that our tracks have an amorphous core that is about 12-14 nm in diameter. This is based on their study of stopping power versus track radius¹⁹, and is expected due to the disruption of the crystal lattice as was described in the ion-solid interactions section. Most of their data was gathered using ion-beam analysis, though they did directly image some of the amorphous tracks using TEM. Because of this result and the fact that amorphous quartz has a lower density than α -quartz, *we expect the crystal lattice to have strain that is radially outward from the track center*. This assumes that an insignificant amount of atoms were ejected from the sample surfaces. Most of our analysis will describe imaging strain contrast in the crystalline quartz around the track, but effects of the amorphous track centerline are also seen and will be discussed as well.

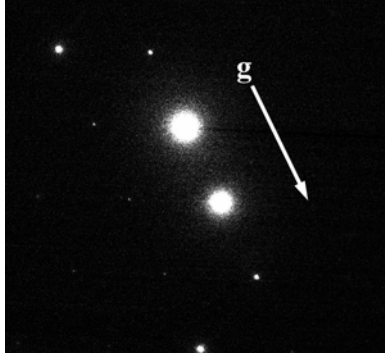


Figure 14: Diffraction pattern showing the (101) 2-beam condition that was used to image the track with the \mathbf{g} -vector perpendicular to the track. Note that there are more than two diffraction spots, but the others are very weak.

6.3 *G-Vector Perpendicular to Track - Exact Bragg Condition*

First, let's examine the case where the \mathbf{g} -vector is perpendicular to the track. For the crystallographic orientation of my specimen, this occurs when using the (110) 2-beam diffraction condition, in which the only bright spots are the direct-beam and the (110) diffracted-beam (**Fig. 14**). In order to set up this condition, I tilted the specimen 21° . I then imaged a track when it was directly on the contour. This is the simplest case to analyze because it is on the exact Bragg condition, which eliminates some complicating factors that will be discussed later. In this case, we expect lattice strain to disrupt the diffraction. This is because lattice strain changes the orientation and lattice spacing of the small crystal volumes around the track, which would take them out of the exact Bragg condition (this is $\mathbf{g} \cdot \mathbf{R}$ contrast). In addition to this, amorphous regions also disrupt diffraction. This is simply due to the fact that electrons are not diffracted from the amorphous region.

Figure 15 shows a bright-field image of a track, with the track being directly on the contour. Note that the sample is tilted by 21° (which is equivalent to saying that the track is tilted 21° from vertical), and that the projection of the track is 32 nm long. Based on geometry, the sample is about 90 nm thick in this region. In bright-field imaging, regions that satisfy the exact Bragg condition are dark, because the diffracted electrons are blocked and do not form the image. This diffracted region forms a contour due to sample bending. First, note that the contrast of the track is essentially symmetric, with the edges of the track being significantly brighter than the center. As discussed in the section on imaging lattice strain, contrast is expected if atoms are displaced in the same direction as the \mathbf{g} -vector. This contrast indicates that there is radial strain. A central feature of this image is that there is a line of no diffraction contrast perpendicular to \mathbf{g} (i.e. along the center of the track). This is expected based on the qualitative kinematical theory of $\mathbf{g} \cdot \mathbf{R}$ contrast. Along the center of the track-line the radial direction is normal to the \mathbf{g} -vector, and contrast is not expected.

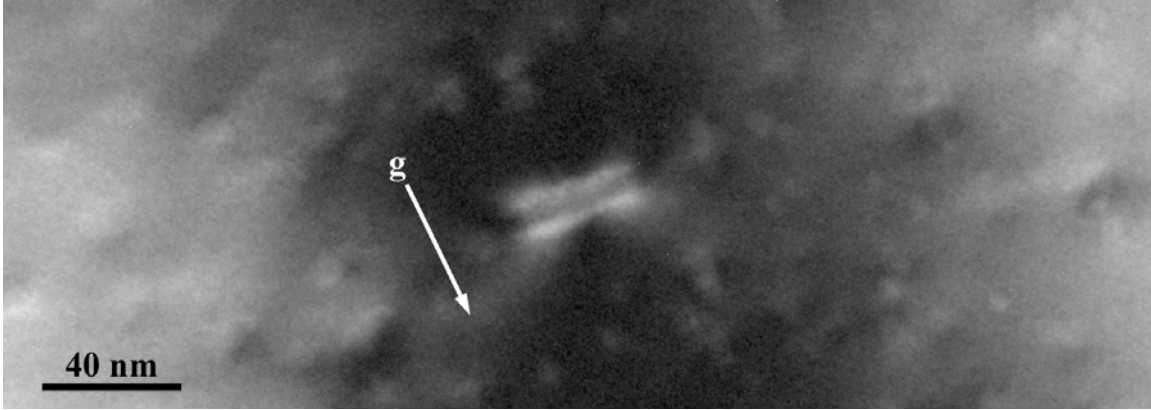


Figure 15: Bright-field TEM image of a track in α -quartz over a contour. The sample is tilted by $\sim 21^\circ$ and it is about 90 nm thick. The dark band passing through the image is a bend contour. This image is the projection of the track. The line of no contrast runs along the center of the track, and the $g \bullet R$ contrast is in the radial direction. The center of the track is not quite as dark as the contour, indicating that the track is amorphous.

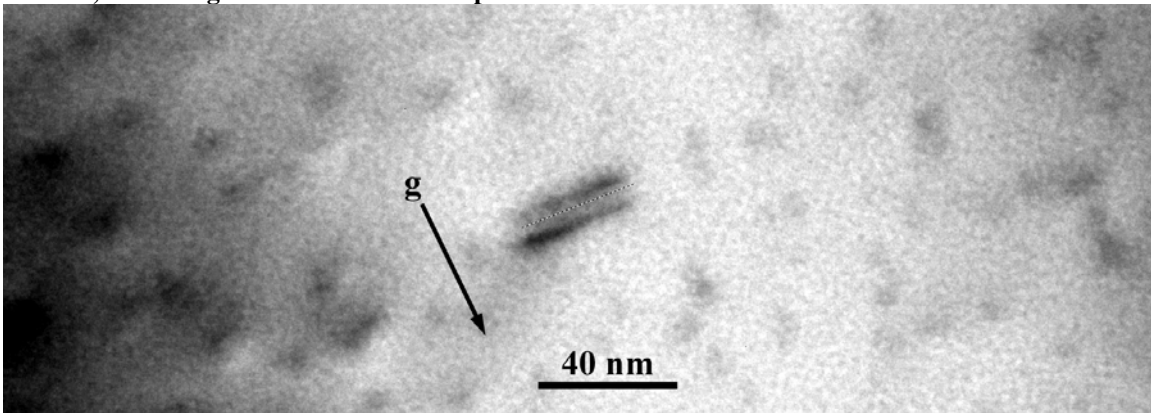


Figure 16: Dark-field image of the same track. The track has the same tilt, and is over the same contour. The only difference is that in figure 15, the diffracted beam was blocked, and here the direct-beam is blocked.

Further, note that the central portion of the track is slightly brighter than the contour. This is consistent with the core of the track being amorphous. Electrons would pass through the amorphous core without diffracting, and thus their intensity would not be removed from the direct beam along the centerline of the track. A measurement of the amorphous region in **Fig. 15** indicates that its diameter is 6 nm. This is only a rough estimate because the exact edge of the amorphous region is blurred due to the strain contrast. In order to determine the exact radius of the amorphous region, it would be necessary to perform high-resolution TEM (HRTEM) using a microscope with higher voltage. We attempted to do HRTEM with our 200 keV microscope, but the quartz was damaged too quickly by the electron beam. Higher energy electrons would damage ionic materials less because their cross-sections are smaller¹⁵. Although this would have been useful to compare to the work of others, it was not necessary because of the large range of data obtained by Meftah et al¹⁸.

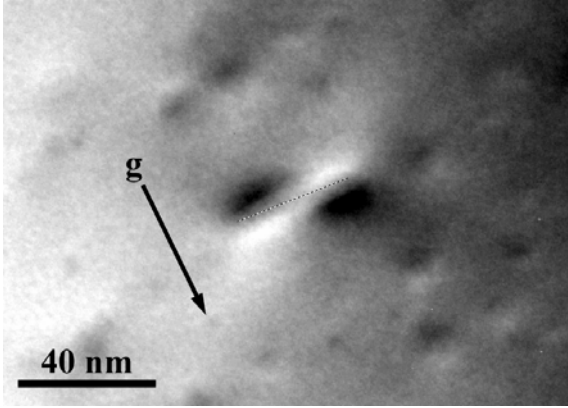


Figure 17: Same track except it is no longer directly over the contour.

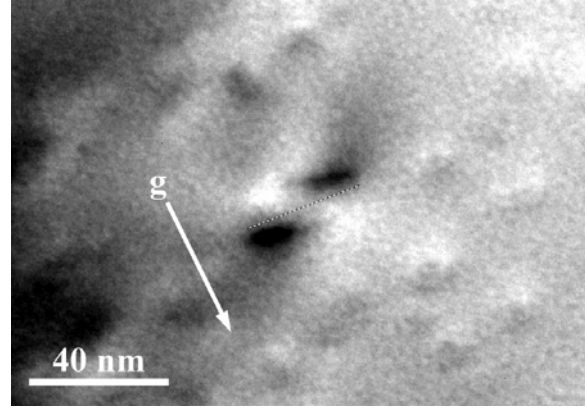


Figure 18: Same track on opposite side of the diffraction contour.

Examining the same track using dark-field imaging (**Fig. 16**) when it is over the contour reveals the same information. In this image, the contrast is reversed because the direct- beam is blocked and the diffracted beam is allowed through to form the image. Now, if a small crystal volume satisfies the Bragg condition, it will be bright, which makes the contour bright. The $\mathbf{g} \bullet \mathbf{R}$ contrast is again in the radial direction, and it is darker than the surroundings because the changed lattice is no longer in the exact Bragg condition. Note that the line of no contrast is again perpendicular to the \mathbf{g} -vector. On close examination, the central track is slightly darker than the surrounding contour, indicating that electrons were not diffracted from it, just as expected for an amorphous core.

6.4 *G-Vector Perpendicular to Track - Near Bragg Condition*

When the *same* track is examined slightly off the Bragg condition, it looks completely different (**Fig. 17**). This difference arises from the complications of imaging near the Bragg condition, instead of at the exact Bragg condition. Though it is very different, there are still two similar features. First, there is still a line of no contrast. In this image a dashed line is drawn through the center of the track. The direction of the dashed line was determined from **Fig. 16**, where it is clear which direction the track projection lies along. A second thing to note is that the contrast is still in the radial direction. Now we must consider the differences. To begin with, the contrast oscillates with depth. Such oscillations in contrast are often seen in TEM, because the intensity of the direct and diffracted plane waves alternate with depth in the material¹⁶. The contrast will thus vary with depth, depending on the intensity of the beams when they reach the small volumes of strained lattice. Another distinct feature of this image is that the contrast is asymmetric across the track line. This is not unexpected because dynamical theory calculations of inclusions with radial strain show such asymmetries¹⁶. Though it would

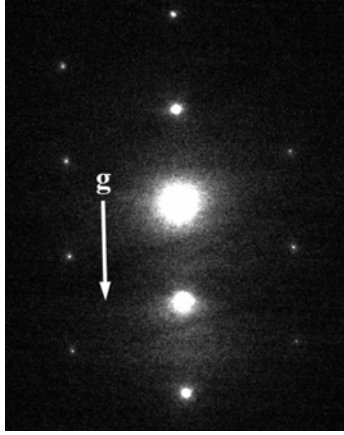


Figure 19: Diffraction pattern of the 2-beam condition that was used to image the new track with the g -vector parallel to the projection of the track. This 2-beam was more difficult to set up, so there are some weaker diffraction spots as well.

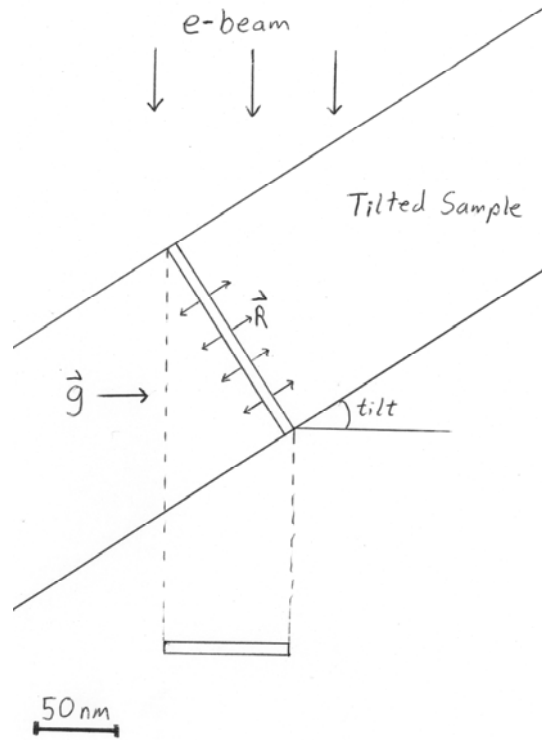


Figure 20: Orientation of sample with respect to the electron-beam. In the projected image $g \bullet R$ appears to be zero, but examining the cross-section view of the sample shows that $g \bullet R$ is not zero along the track (in the plane of the drawing), but it is zero to the sides (normal to the drawing).

be very complicated to calculate what would happen for our exact case, we can still learn from this asymmetry. On one side of the track center, the lattice strain bends the atomic planes so that they are closer to the Bragg condition, and on the other side it bends them so that they are further away. This is to be expected because the lattice is strained in opposite directions on the two sides. **Figure 17** shows the track to one side of the (110)-contour, and **Fig. 18** shows it on the other side. As can be seen, the contrast reverses. This is further evidence that the strain on one side of the track center brings the lattice closer to the Bragg condition, and the strain on the other side takes it further away.

6.5 *G-vector Parallel to Track - Exact Bragg Condition*

Now, let's tilt the specimen to a new orientation and examine tracks with the (100) g -vector, which is parallel to the tracks (**Fig. 19**). In fact, it is only parallel when looking in projection. As shown in **Fig. 20**, this new track is actually at an angle with respect to the

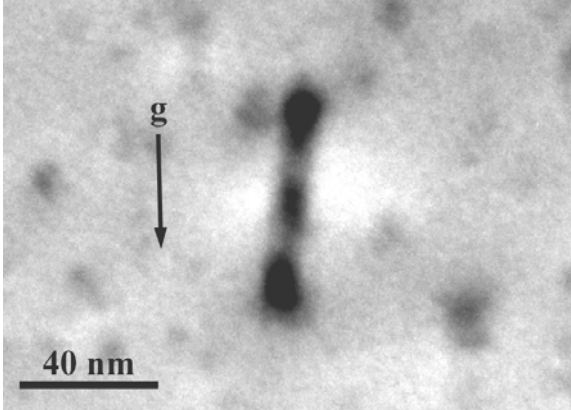


Figure 21: Dark-field image of a new track over contour. The sample is tilted by 25° and is about 160 nm thick in this area. The track is oriented differently than the previous one because a different tilt was used. With this \mathbf{g} -vector, the contrast is along the direction of the track.

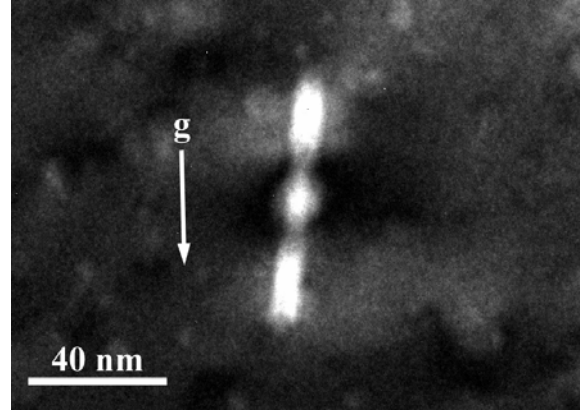


Figure 22: Bright-field image of the same track over the contour.

horizontal. **Figure 21** shows a dark-field image of a new track that was imaged with the (100) 2-beam condition. This track was found in a thicker area. The total tilt is about 25° , and the projected length is 65 nm. By geometry, the thickness of the sample in this region is about 160 nm, almost twice as thick as the previous region. The reason for this is that it is hard to determine how thick the area is before you find a track, and it was not thought to be important. As can be seen, there is contrast along the central part of the track, but there is little contrast toward the outside. This can again be explained using the same track model and the kinematical theory. At the sides of the track, the atom displacement is perpendicular to the \mathbf{g} -vector. At the very center of the track $\mathbf{g} \cdot \mathbf{R}$ is not zero, which can be seen by examining **Fig. 21**. So in the projected image, the most $\mathbf{g} \cdot \mathbf{R}$ contrast will be at the center of the track, and it will fade away toward the edge of the track. The amorphous cylinder is not easily seen because the intense $\mathbf{g} \cdot \mathbf{R}$ contrast covers it up.

The bright-field image taken with the track over a contour shows the same features with the contrast reversed (**Fig. 22**). This contrast reversal is expected for an ideal 2-beam condition since electrons are either in the transmitted beam or in the diffracted beam. In this image as well as in the previous one, the contrast oscillates with depth. This is likely due to the thickness effects that were described for the other track. The reason why they are now visible when over the contour is likely due to the increased length of the track. In **Fig. 15** there may also be intensity variations, but because the track is not very long they are not apparent.

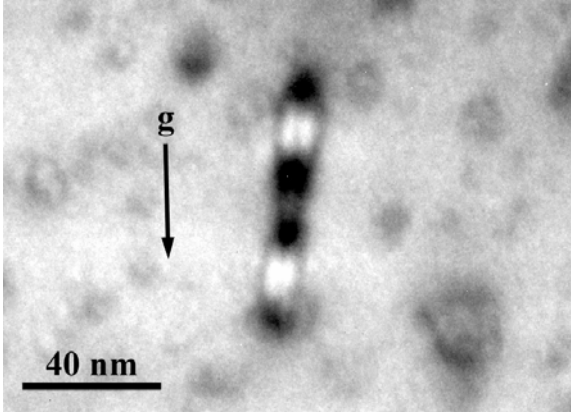


Figure 23: Bright-field image of same track. It is no longer directly over the contour, and is imaged slightly underfocus.

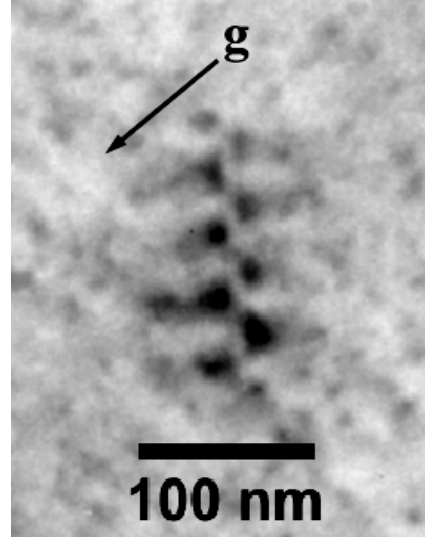


Figure 24: Same image as is in Fig. 2, except the g-vector is added. The track has a combination of the contrast that we saw for the g-vector perpendicular and parallel to the track. The perpendicular component is dominant, but there is a contrast oscillation along the track as well. The track is ~250nm thick, which accounts for so many oscillations.

6.6 *G-vector Parallel to Track - Near Bragg Condition*

Fig. 23 shows the same track when it is tilted away from the exact Bragg condition. With this imaging condition, the contrast is along the track center and it oscillates with depth. These features are similar to those seen when the track was directly over the contour. The contrast oscillations along the track are likely due to the sample thickness. The contrast along the track center is expected from our model. This image was taken with a slight underfocus. This underfocus introduces Fresnel contrast, which is sensitive to atomic density and produces a dark line at the amorphous - crystalline boundary¹⁵. Using this contrast, I measured an amorphous track diameter of 8 nm. Because of the strain contrast, it was still difficult to measure the diameter of the amorphous cylinder.

7 Conclusion

The goal of this project was to understand the structure of the rather complicated track diffraction contrast seen in Fig. 2. After much complicated analysis, it appears that the simplest explanation is correct: the high-energy ions produce lower density amorphous cylinders, which thus place a radial strain on the crystalline lattice.

Other tracks imaged with the two conditions just described above had the same distinctive features. However, they did not look exactly the same, due to irregularities in the sample's surfaces. For increased clarity, I chose to show the tracks that were located in regions with the least sample damage.

When imaging using other **g**-vectors, the contrast appears to be a combination of the two examined cases, which is to be expected. As can be seen in **Fig. 24**, the **g**-vector is at an angle with respect to the track, and contrast is seen in the radial direction and along the track centerline.

Examining the radius of the amorphous track using the different imaging conditions, it appears that their radius is 6-8 nm. This is a rough estimate due to the ambiguity caused by the diffraction contrast. Note that this is less than the 12 nm value estimated from the data of Meftah et al¹⁸.

8 Acknowledgements

This research project would not have been possible without the help of many people. I would like to thank the following individuals: David Follstaedt for teaching me transmission electron microscopy, and for helping me analyze the track contrast; Barney Doyle for giving me the opportunity to perform this research, and for helping me understand ion-solid interactions and accelerator physics; David Dunlap for helpful discussions about the project and the theory; Mike Moran for teaching me everything I know about preparing excellent TEM samples; Dan Buller (SNL) for operating the accelerator and for showing me how it works; Del McDaniel (University of North Texas) for bringing our RFQ into operation; Paolo Rossi (Università di Padova, Italy) for helping me understand ion-solid interactions; and Eduardo Bringa (LLNL) for explaining his molecular dynamics simulations to me.

Sandia is a multiprogram laboratory operated by Sandia Corporation, a Lockheed Martin Company, for the United States Department of Energy's National Nuclear Security Administration under Contract DE-AC04-94AL85000.

References

- ¹ D.M. Follstaedt, A.K. Norman, P. Rossi, B.L. Doyle, F.D. McDaniel and E.M. Bringa, Proceedings of the International Conference on Ion Beam Modification of Materials 2004, to be published in Nuclear Instruments and Methods B.
- ² F. Seitz, Discuss. Faraday Soc. **5** (1949) 271.
- ³ A. Meftah et al., Phys. Rev. B 49 (1994), 12457.
- ⁴ R. L. Fleischer, P. B. Price and R. M. Walker, J. Appl. Phys. 36 (1965) 3645; R. L. Fleischer et al., Phys. Rev. 156 (1967) 353.
- ⁵ E. M. Bringa and R. E. Johnson, Phys. Rev. Lett. **88** (2002) 165501.
- ⁶ A. Meftah et al., Phys. Rev. B 49 (1994), 12457.
- ⁷ J.F. Ziegler, J.P. Biersack and U. Littmark, in: The Stopping and Range of Ions in Solids (Pergamon, 1985). This data was compiled into a program called SRIM and I used version 2003.26.
- ⁸ http://www.accsys.com/about/history_p3.html, 3/8/05
- ⁹ <http://www.touchscreens.com/intro-touchtypes-saw.html>, 4/2005
- ¹⁰ http://www.sawyerresearch.com/Qtz_MSDS.htm, 2/8/2005
- ¹¹ B. Vainshtein, V.M. Fridkin, V.L. Indenbom, "Structure of Crystals", Third Revised edition, Springer, pg 144.
- ¹² International Centre For Diffraction Data, Newton Square, PA 19073-3273, Card # 5-0490.
- ¹³ <http://webmineral.com/data/Lechatelierite.shtml>, 2/10/05
- ¹⁴ The four diffraction pattern zones that we identified were: [2 -2 2], [2 -2 3], [2 -2 4] and [2 -2 6].
- ¹⁵ D.B. Williams, C.B. Carter, "Transmission Electron Microscopy", Plenum Press, 1996. See page 101 for TEM resolution, page 63 for sample damage, and page 405 for strain contrast.
- ¹⁶ P. Hirsch et al "Electron Microscopy of Thin Crystals", Robert E. Krieger Publishing Company, 1977. See page 156 for the kinematical theory, page 195 for the dynamical theory, page 159 for depth contrast oscillations, and page 202 for asymmetry examples.
- ¹⁷ M.R. Pascucci, J.L. Hutchison, L.W. Hobbs, Radiation Effects **74** (1983), 219.
- ¹⁸ A. Meftah et al., Phys. Rev. B 49 (1994), 12457. See Table 12.1.
- ¹⁹ Other factors such as ion mass and charge are less important, though the fraction of energy deposited out to a certain radius can change slightly.